

# Anion photoelectron spectroscopy of $I_2^-$ and $I_2^- \cdot Ar_n$ ( $n=1-14, 16, 20$ ) clusters

Knut R. Asmis, Travis R. Taylor, Cangshan Xu, and Daniel M. Neumark

*Department of Chemistry, University of California, Berkeley, California 94720*

(Received 5 February 1998; accepted 15 June 1998)

We report the mass-selected anion photoelectron spectra of  $I_2^-$  and the weakly bound clusters  $I_2^- \cdot Ar_n$  ( $n=1-14, 16, 20$ ) measured at a photon energy of 4.657 eV. The experiment yields size-dependent vertical and adiabatic detachment energies for the formation of the ground state and five valence-excited states of the neutral cluster, which correspond to the  $^1\Sigma_g^+$  ( $X$ ),  $^3\Pi_{2u}$  ( $A'$ ),  $^3\Pi_{1u}$  ( $A$ ),  $^3\Pi_{0-u}$  ( $B'$ ),  $^1\Pi_{1u}$  ( $B''$ ), and  $^3\Pi_{0+u}$  ( $B$ ) states of bare  $I_2$ . The detachment energies are successively blue-shifted with increasing cluster size, indicating a stronger stabilization of the anionic cluster relative to the neutral counterpart. The blue shift is of similar extent for the electronically excited states  $A'$  and  $A$  and approximately 10% less for the  $X$  state. The  $I_2^-$  and  $I_2^- \cdot Ar$  spectra are simulated employing a Franck-Condon analysis, from which we estimate the ion vibrational temperature and determine the  $I_2^- - Ar$  binding energy ( $D_0 = 53 \pm 4$  meV). The results are discussed with respect to possible cluster geometries and the evolution of the total and stepwise solvation energies. For  $I_2^- \cdot Ar_6$  we present evidence that all Ar atoms are bound around the waist of the I-I bond. © 1998 American Institute of Physics. [S0021-9606(98)02935-3]

## I. INTRODUCTION

Weakly bound clusters involving a solvated chromophore provide an interesting and challenging research field, due to their unique role as a form of matter with properties intermediate between the gas phase and condensed phase limits. In this context, one is generally interested in characterizing the forces that are responsible for changes in the properties of the solute upon its stepwise solvation. The halogen molecule-rare gas system has proven to be particularly suitable for these studies, because of its relative simplicity, i.e., a system comprising a spectroscopically well characterized homonuclear diatomic weakly interacting with inert rare gas atoms. The  $I_2 \cdot Ar_n$  ( $n=1,2,3,\dots$ ) system has received particular attention. Early spectroscopic studies of complexes of  $I_2$  with rare gas atoms have been reviewed by Levy.<sup>1</sup> The more recent experimental<sup>2-6</sup> and theoretical<sup>7-13</sup> studies on  $I_2 \cdot Ar_n$  clusters have concentrated on the characterization of the solvent induced geminate recombination of  $I_2$  upon photodissociation, referred to as the "cage" effect.

A parallel and more recent effort has focused on weakly bound ionic clusters.<sup>14</sup> A particularly useful technique for examining the energetics of clusters *size selectively* is anion photoelectron spectroscopy. Here a mixture of cluster anions is generated, mass selected, and then photodetached, effectively probing changes in the solute-solvent interaction between the anion and the neutral as a function of cluster size. Detailed information on binding energies and solvation geometries can be extracted from these experiments as shown in the studies of Cheshnovsky and coworkers<sup>15-18</sup> on halide anions solvated in  $CO_2$  and  $H_2O$  clusters and of Bowen and co-workers<sup>19</sup> on  $O^- \cdot Ar_n$ . Furthermore, anion photoelectron spectroscopy can be employed as an alternative to mass-selected two-color photoionization experiments<sup>20-23</sup> for the study of matrix shifts in molecular electronic transitions of

neutral clusters. Research in our group includes studies on  $X^- \cdot (CO_2)_n$ ,  $X^- \cdot (N_2O)_n$ , and  $X^- \cdot Ar_n$  ( $X^- = Cl^-, Br^-,$  and  $I^-$ ).<sup>24-27</sup> In this article we extend our studies on halide-rare gas systems to include clusters involving a molecular chromophore, the diatomic species  $I_2^-$ . We apply anion photoelectron spectroscopy to focus on the energetics of the  $I_2^- \cdot Ar_n$  system.

This study has been stimulated by recent experimental<sup>28-31</sup> and theoretical<sup>32-34</sup> studies on the dynamical behavior of  $I_2^- \cdot Ar_n$  clusters upon photoexcitation. Lineberger and co-workers have performed a series of photodissociation experiments on  $I_2^- \cdot Ar_n$  clusters in order to determine the dependence of the  $I_2^-$  caging yield with cluster size as well as the overall time scale for recombination and vibrational relaxation of the  $I_2^-$  chromophore.<sup>28,29</sup> Their work is a continuation of their elegant studies on the photofragmentation of  $I_2^- \cdot (CO_2)_n$  and  $Br_2^- \cdot (CO_2)_n$ .<sup>35-39</sup> Our group has recently applied femtosecond anion photoelectron spectroscopy to study the time-resolved photodissociation dynamics of  $I_2^- \cdot (Ar)_n$  clusters.<sup>30,31</sup> Nonadiabatic molecular dynamics simulations reproduce many of the features seen in the photodissociation and FPES experiments.<sup>32-34</sup> However, the interpretation of the dynamics experiments is still somewhat limited by the absence of spectroscopic information on the anion clusters. In particular, one would like to know the cluster geometries and the solvation energies as a function of size. Calculations of these properties can be problematic, as evidenced by two rather different structures calculated recently for  $I_2^- \cdot Ar_6$ ; in one,<sup>32</sup> the  $I_2^-$  is bound to the surface of an  $Ar_6$  cluster, and in the other,<sup>33</sup> the six Ar atoms form a ring around the  $I_2^-$  bond.

In the present study we address these issues by measuring the anion photoelectron spectra of  $I_2^-$  and  $I_2^- \cdot Ar_n$  clusters ( $n=1-14, 16, 20$ ). We describe the experimental setup and

the source conditions for the production of  $I_2^- \cdot Ar_n$  clusters. We then present the anion photoelectron spectra. The  $I_2^-$  and  $I_2^- \cdot Ar$  spectra are simulated employing a Franck–Condon analysis, from which we estimate the ion vibration temperature and determine the  $I_2^- \cdot Ar$  binding energy. This analysis makes use of our recently reported potential for the  $I_2^-$  ground state.<sup>40</sup> The observed shifts of the bands in the photoelectron spectra upon increasing degree of solvation are discussed in terms of changes in cluster solvation energy as a function of cluster size and electronic state. Among other things, these shifts yield the  $I_2^- \cdot Ar$  binding energy and support the “solvent ring” geometry for  $I_2^- \cdot Ar_6$ .

## II. EXPERIMENT

The negative ion time-of-flight (TOF) photoelectron spectrometer used in this study has been described in detail previously<sup>41,42</sup> and only the salient features will be given here.  $I_2^- \cdot Ar_n$  clusters are prepared by coexpanding iodine vapor with 4–20 psi of Ar at room temperature through a pulsed molecular beam valve (0.75 mm diameter orifice), operating at 20 Hz. A 1 keV, 300  $\mu A$  electron beam crosses the gas jet just outside the nozzle, in the continuum flow region of the expansion. The negative ions formed in the supersonic expansion are cooled internally and extracted perpendicularly to the expansion by means of a pulsed electric field. They are then accelerated to a beam energy of 3.75 keV and enter a linear reflection TOF mass spectrometer. The extracted ions separate in time and space according to their mass to charge ratios and are detected at the end of the flight tube by a pair of 25 mm diameter chevron-mounted microchannel plates. The mass resolution is  $m/\Delta m \approx 2000$ .

Photoelectrons are detached from the mass-selected ions by a fixed frequency laser pulse from a Nd:YAG laser operated at 20 Hz. The laser firing delay is varied until optimal temporal overlap is achieved with the ion of interest. The fourth harmonic (266 nm, 4.657 eV) of the Nd:YAG laser was used in the present study. The angle between the laser polarization and the direction of electron collection can be varied by means of a half-wave plate. All spectra reported here were measured at a laser polarization angle of  $\theta = 90^\circ$ .

The photoelectron kinetic energy is determined by time-of-flight. The detached electrons are detected at the end of a 1 m magnetically shielded flight tube, mounted orthogonal to the laser and ion beam. The electron detector covers a solid angle of 0.0013 sr, i.e., 0.01% of the detached photoelectrons are detected. The instrumental resolution is 8–10 meV for an electron kinetic energy (eKE) of 0.65 eV and degrades as  $(eKE)^{3/2}$ . Under typical conditions, the ion density in the laser interaction region is about  $10^5/cm^3$  for  $I_2^-$  and decreases with increasing cluster size. Around 30% of the ions are photodetached at 266 nm and about one electron is detected per laser shot. A typical spectrum requires 300 000–600 000 laser shots. Ultraviolet photons efficiently eject electrons from metal surfaces, resulting in a residual background photoelectron contribution of typically one electron per ten laser shots at 266 nm, primarily at low eKE. Background spectra

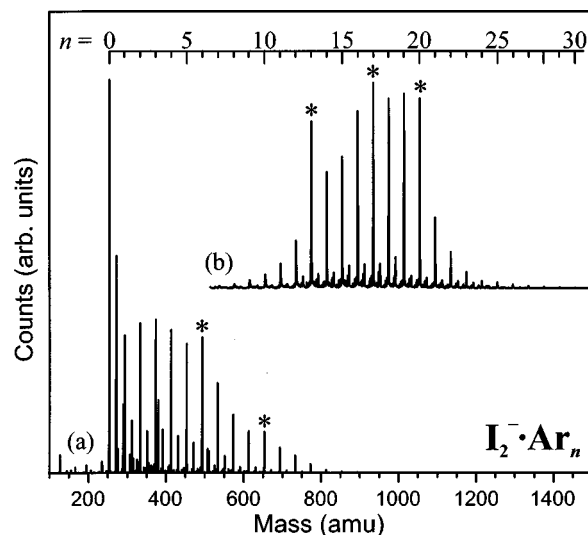


FIG. 1. Mass spectra of the  $I_2^- \cdot Ar_n$  clusters: (a) instrument optimized for low  $n$ , (b) instrument optimized for higher  $n$ . Magic number clusters are marked with an asterisk (\*).

were recorded on a daily basis, summed, and then subtracted from the acquired data.

All photoelectron spectra presented here are plotted as a function of the electron kinetic energy eKE (bottom axis) and the electron binding energy eBE (top axis), which is defined as

$$eBE = h\nu - eKE, \quad (1)$$

where  $h\nu$  denotes the photon energy of the detachment laser.

## III. RESULTS

Two representative mass spectra of the  $I_2^- \cdot Ar_n$  clusters formed in our source are shown in Fig. 1. The spectra were measured under conditions optimized for smaller (a) and larger (b) clusters. The most intense peak in spectrum (a) is due to  $I_2^-$ , followed by a progression of peaks spaced by 40 mass units.  $I_2^- \cdot Ar_{30}$  was the largest cluster observed in this study, but clusters with  $n > 20$  were formed in insufficient quantity to permit acquisition of photoelectron spectra with the current experimental setup. Magic numbers in the mass spectra occur at  $n = 6, 10, 13,$  and  $20$  and are generally attributed to clusters with higher relative stability. The weaker features between the  $I_2^- \cdot Ar_n$  peaks are predominantly due to the formation of clusters of the type  $I_x^- \cdot Ar_n$  ( $x = 3, 4, 5$ ) and  $I_2^- \cdot Ar_n \cdot H_2O$ . Throughout the course of the study the presence of small amounts of water, possibly initially adsorbed to the metal inlet system, proved to be essential for the formation of sufficient amounts of larger  $I_2^- \cdot Ar_n$  clusters. Our mass spectra have considerably less unresolved background signal compared to those reported previously by Vorsa *et al.*<sup>28</sup> The main spectral features are nonetheless similar, reflecting similar ion production conditions in the two experiments.

The anion photoelectron spectrum of  $I_2^-$  measured at a photodetachment wavelength of 266 nm is shown in Fig. 2. Six bands are observed centered at eKEs of 1.422 eV (X), 0.875 eV (A'), 0.783 eV (A), 0.533 eV (B'), 0.422 eV

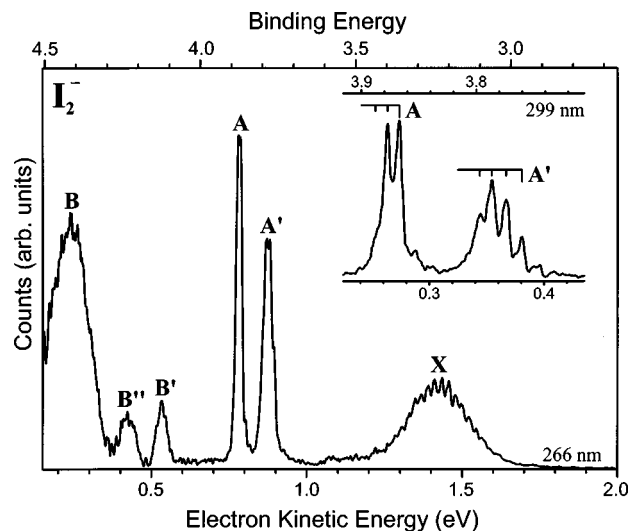


FIG. 2. Anion photoelectron spectrum of  $I_2^-$  measured at a photon energy of 4.657 eV, corresponding to a photon wavelength of 266 nm. An excerpt of the previously reported  $I_2^-$  spectrum (Ref. 40) measured at 4.141 eV (299 nm) is shown in the top right corner.

( $B''$ ), and 0.239 eV ( $B$ ). The  $X$ ,  $A'$ , and  $A$  bands exhibit vibrational structure. This structure is considerably less pronounced than in the previously reported 299 nm anion photoelectron spectrum<sup>40</sup> of  $I_2^-$ , an excerpt of which is shown in the top right corner of Fig. 2. This is due to the higher photon energy employed in the current study, resulting in a higher kinetic energy of the corresponding photoelectrons and thus lower energy resolution of the TOF electron analyzer. However, the higher photon energy leads to the observation of three additional unstructured bands  $B'$ ,  $B''$ , and  $B$  at low eKEs. We assign the observed bands to the transitions from the anion ground state ( $^2\Sigma_u^+$ ) to the ground state and five valence excited states of  $I_2$ :  $^1\Sigma_g^+$  ( $X$ ),  $^3\Pi_{2u}$  ( $A'$ ),  $^3\Pi_{1u}$  ( $A$ ),  $^3\Pi_{0-u}$  ( $B'$ ),  $^1\Pi_{1u}$  ( $B''$ ), and  $^3\Pi_{0+u}$  ( $B$ ). This assignment is based on previously determined potential energy curves for the  $I_2^-$  ground state<sup>40</sup> and the ground and valence excited states<sup>43–45</sup> of neutral  $I_2$ .

The 266 nm anion photoelectron spectra of  $I_2^-$  and  $I_2^- \cdot Ar_n$  ( $n=1-14, 16$ , and  $20$ ) are shown in Fig. 3. Comparison of the  $I_2^- \cdot Ar$  spectrum to that of  $I_2^-$  (see also Fig. 4) shows that all bands are shifted to lower eKEs by 21–26 meV. Band  $X$  in the  $I_2^-$  spectrum extends to higher and lower eKE than the corresponding band in the  $I_2^- \cdot Ar$  spectrum, and in general all bands in the  $I_2^-$  spectrum are slightly broader. This effect, discussed below, is due to vibrational hot bands in the bare anion. The spectra of the larger  $I_2^- \cdot Ar_n$  clusters remain similar in form, except for a continuous shift of the bands to lower eKEs. The signal-to-noise ratio decreases with increasing cluster size due to lower ion signal. Nonetheless, the band envelopes and widths are approximately constant for the  $I_2^- \cdot Ar_n$  ( $n \geq 1$ ) spectra.

All bands are successively shifted to lower eKEs, i.e., higher electron binding energies, with increasing cluster size. The  $X$ ,  $A'$ , and  $A$  bands appear in the spectra up to  $n=20$ . The weaker  $B'$  and  $B''$  bands are observed only up to  $n=4$ , after which the signal-to-noise ratio at low eKE de-

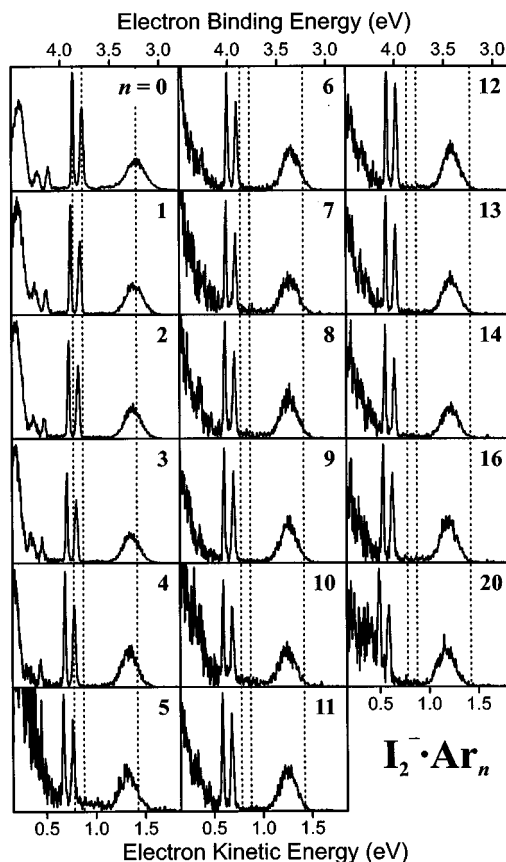


FIG. 3. Anion photoelectron spectra of  $I_2^- \cdot Ar_n$  clusters measured at a photon energy of 4.657 eV. The vertical detachment energies for the formation of the  $X$ ,  $A'$ , and  $A$  states of bare  $I_2^-$  are indicated by the broken vertical lines.

creases to the point where they cannot be clearly observed. The  $B$  band is shifted above the photodetachment threshold with increasing cluster size. The maximum of the  $B$  band can be seen up to  $n=3$ , but lies in the region of the spectrum which is most sensitive to the background subtraction, thus lowering the accuracy with which we can determine its position.

The total and stepwise band shifts for each of the six bands are listed in Table I. These shifts are determined by horizontally displacing the band of interest to achieve best overlap with the corresponding feature in the  $I_2^- \cdot Ar$  spectrum. We find this method to be more accurate for the determination of the band shifts as opposed to estimating the position of the band maximum. The stepwise shift, i.e., the shift per added Ar atom, is given in parentheses. In those cases where the stepwise shift cannot be determined directly ( $n=16$  and  $20$ ), because the  $n-1$  spectrum was not measured, the averaged stepwise shift is given. The relative energies determined in this way are accurate within  $\pm 4$  meV for the  $A$ ,  $A'$ , and  $B'$  bands and  $\pm 10$  meV for the  $X$ ,  $B''$ , and  $B$  bands. The total shift increases monotonically for all observed bands. The  $A$  band is shifted by 25 meV by the first Ar atom. The next five Ar atoms shift the band by another 20–23 meV each, after which the stepwise shift is considerably reduced by roughly 50% and remains between 10–14 meV up to  $n=20$ . A similar trend is observed for the  $A'$  and  $X$  band. The stepwise shift per Ar atom for the  $X$  band is

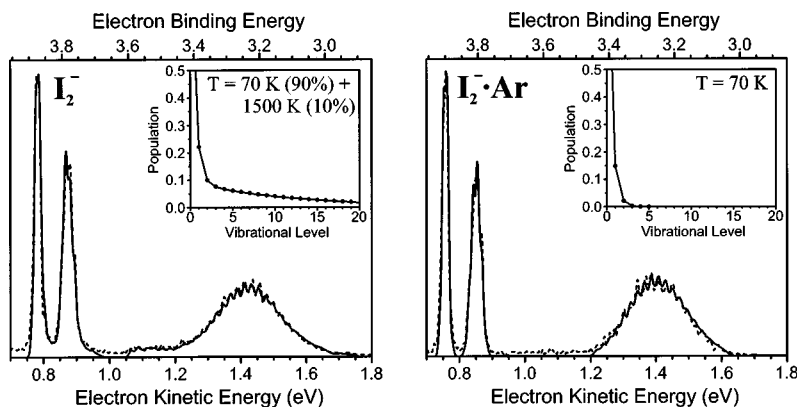


FIG. 4. Experimental (dashed) and simulated (solid) photoelectron spectra of  $I_2^-$  and  $I_2^- \cdot Ar$ . The populations of the vibrational levels assumed for the Franck-Condon fit are shown in the top right corner.

consistently smaller than for the  $A'$  and  $A$  bands. The shifts of the  $B'$ ,  $B''$ , and  $B$  bands can only be determined with lower accuracy and up to lower cluster size, but appear to be comparable to the shifts of the other bands in the same size range.

#### IV. ANALYSIS

##### A. Detachment energies

The vertical detachment energy (VDE) is defined as the electron binding energy at the band maximum. The VDEs for  $I_2^-$  are 3.235 eV ( $X$ ), 3.782 eV ( $A'$ ), 3.874 eV ( $A$ ), 4.124 eV ( $B'$ ), 4.235 eV ( $B''$ ), and 4.418 eV ( $B$ ). We do not state the VDEs for all the clusters studied explicitly in this report, but they can easily be determined by adding the tabulated shifts (Table I) to the VDEs of bare  $I_2^-$ . The adiabatic detachment energy (ADE) refers to the transition between the vibrational ground states and is also called the electron affinity when the final state is the electronic ground state of the neutral cluster. ADEs can often not be determined by inspection of the photoelectron spectrum, but, as shown below, they can be determined for transitions to the  $X$ ,  $A'$ , and  $A$  states in the  $I_2^-$  and  $I_2^- \cdot Ar$  spectra using a Franck-Condon

analysis. The band contours associated with these states remain essentially unchanged throughout the spectra. We thus assume the energy gap between the VDE and the corresponding ADE remains approximately constant and the ADEs for all clusters can be determined in a similar fashion as described for the VDEs, i.e., by adding the shifts listed in Table I to the corresponding ADEs of  $I_2^-$ .

##### B. Franck-Condon analysis

We have performed a Franck-Condon analysis for the anion photoelectron spectra of  $I_2^-$  and  $I_2^- \cdot Ar$  in order to determine the ADEs of the  $X$ ,  $A'$ , and  $A$  states and characterize the vibrational temperature of the negative ions. The procedure employed here has been described previously by Zanni *et al.* in their 299 nm photoelectron study of  $I_2^-$ .<sup>40</sup> In the analysis of the  $I_2^- \cdot Ar$  spectrum we neglect any excitation of the van der Waals modes, a reasonable assumption given that the bands in the  $I_2^- \cdot Ar$  spectrum are narrower than in the  $I_2^-$  spectrum. Rydberg-Klein-Rees potentials determined from fluorescence measurements are used for the electronic states of neutral  $I_2$ .<sup>46-48</sup> For the anion electronic ground state we employed the previously determined Morse potential.<sup>40</sup> We

TABLE I. Total and stepwise shift (in parentheses) of the bands in the photoelectron spectra of  $I_2^- \cdot Ar_n$  clusters relative to the  $I_2^-$  spectrum as a function of cluster size  $n$ . All energies are in meV.

$n$	$X(^1\Sigma_g^+)$	$A'(^3\Pi_{2u})$	$A(^3\Pi_{1u})$	$B'(^3\Pi_{0-u})$	$B''(^1\Pi_{1u})$	$B(^3\Pi_{0+u})$
0	0	0	0	0	0	0
1	24 (+24)	26 (+26)	25 (+25)	25 (+25)	26 (+26)	21 (+21)
2	46 (+22)	49 (+23)	48 (+23)	48 (+23)	46 (+20)	42 (+21)
3	68 (+22)	71 (+22)	70 (+22)	71 (+23)	69 (+23)	
4	89 (+21)	93 (+22)	92 (+22)	91 (+20)		
5	109 (+20)	114 (+21)	113 (+21)			
6	129 (+20)	134 (+20)	133 (+20)			
7	142 (+13)	147 (+13)	147 (+14)			
8	154 (+12)	160 (+13)	160 (+13)			
9	164 (+10)	173 (+13)	173 (+13)			
10	174 (+10)	186 (+13)	185 (+12)			
11	183 (+9)	196 (+10)	195 (+10)			
12	192 (+9)	206 (+10)	205 (+10)			
13	200 (+8)	216 (+10)	216 (+11)			
14	210 (+10)	228 (+12)	228 (+12)			
16 <sup>a</sup>	228 (+9)	251 (+12)	251 (+12)			
20 <sup>a</sup>	261 (+8)	292 (+10)	291 (+10)			

<sup>a</sup>Averaged stepwise shifts.

TABLE II. Results of the Franck–Condon analysis of the anion photoelectron spectra of  $I_2^-$  and  $I_2^- \cdot Ar$ . The vibrational temperature  $T$  (in K, see text), the I–I equilibrium distance  $R_{eq}$  (in Å), the electron affinity (EA) and the adiabatic detachment energies (ADEs) are listed. All energies are in meV.

	$T$	$R_{eq}$	EA	$ADE^{A' \text{ state}}$	$ADE^{A \text{ state}}$
$I_2^-$	70 (1.0), 1500(0.1)	3.205	2.524	3.763	3.869
$I_2^- \cdot Ar$	70 (1.0)	3.203	2.548	3.789	3.894

then varied the population of the vibrational levels and band origins to achieve the best fit with the experimental spectra.

The simulated spectra are shown in Fig. 4 and the results are listed in Table II. The ADEs for  $I_2^-$  are 2.524 (X), 3.763 (A'), and 3.869 eV (A) and are blue-shifted in  $I_2^- \cdot Ar$  by 24, 26, and 25 meV, respectively, to 2.548, 3.789, and 3.894 eV. Note that the shifts determined in this fashion and those taken from Table I, which refer to the shifts in the VDE, are identical. While a minor reduction of the I–I bond length in  $I_2^- \cdot Ar$  (0.002 Å) is necessary to obtain the best fit, the band profiles in the  $I_2^- \cdot Ar$  spectrum are well reproduced within our simple model.

The populations of the anion vibrational levels are shown in the top right corner of each spectrum. The population is approximated in terms of Boltzmann distributions, each characterized by a mean temperature and a weighting factor. The changes in band contours between the  $I_2^-$  and  $I_2^- \cdot Ar$  spectra are due to a drastic decrease in the ion vibrational temperature. For the  $I_2^-$  spectrum the high temperature component, even though it contributes only 10% to the distribution, is solely responsible for the pronounced low eKE tail of the X band and the high eKE tails of the X, A', and A bands. A single Boltzmann distribution with an average temperature of 70 K was sufficient to fit the  $I_2^- \cdot Ar$  spectrum.

The considerable decrease in the vibrational temperature distribution of  $I_2^- \cdot Ar$  relative to  $I_2^-$  can be accounted for by an evaporative cooling mechanism. Taking the  $I_2^- \cdot Ar$  binding energy (see discussion section) and the vibrational frequency ( $110 \text{ cm}^{-1}$ )<sup>30</sup> of  $I_2^-$  into account an energy corresponding to at least four vibrational quanta of the  $I_2^-$  stretch vibration is sufficient for the breaking of the van der Waals bond. From previous results it is known that the time scale for vibrational predissociation lies in the picosecond domain,<sup>29,31</sup> enabling the higher vibrationally excited  $I_2^- \cdot Ar$  clusters to efficiently decay into  $I_2^-$  and Ar before they reach the extraction region. Therefore the vast majority of the  $I_2^- \cdot Ar$  clusters probed will have less than four quanta of  $I_2^-$  excitation. No comparable mechanism is available to  $I_2^-$  and thus “hotter”  $I_2^-$  can remain in the beam.

### C. Solvation energies

In order to stay consistent with previous anion photoelectron studies we adopt the terminology of Arnold *et al.*<sup>19</sup> and relate the energetic information obtained from the photoelectron spectra to the total and stepwise solvation energies of the ionic and the neutral clusters. Based on our previous experience with halogen atom-rare gas clusters<sup>27</sup> we explicitly include the solvation energy of the neutral cluster, since we expect it to be non-negligible compared to the solvation

energy of the corresponding charged cluster. The stepwise solvation energies  $SE_{\text{step}}^i(n)$  and  $SE_{\text{step}}^-(n)$  are defined as the solvent dissociation energies for the loss of a single Ar atom from  $I_2 \cdot Ar_n$  or  $I_2^- \cdot Ar_n$ , respectively; the superscript  $i$  indicates the  $I_2$  neutral electronic state. The total solvation energy  $SE_{\text{tot}}(n)$ , defined for the anion and neutral clusters, is given by the sum over the stepwise solvation energies  $SE_{\text{step}}(x)$ :

$$SE_{\text{tot}}(n) = \sum_{x=1}^n SE_{\text{step}}(x). \quad (2)$$

The ADEs are related to the stepwise solvation energy difference  $\Delta SE_{\text{step}}^i(n)$ , i.e., the difference in the stepwise solvation energy of the neutral,  $SE_{\text{step}}^i(n)$ , and of the anionic cluster,  $SE_{\text{step}}^-(n)$ , as follows:

$$\begin{aligned} ADE^i(n) - ADE^i(n-1) &= SE_{\text{step}}^-(n) - SE_{\text{step}}^i(n) \\ &\equiv \Delta SE_{\text{step}}^i(n). \end{aligned} \quad (3)$$

The total solvation energy difference  $\Delta SE_{\text{tot}}^i(n)$  is then given by:

$$ADE^i(n) - ADE^i(0) = \sum_{x=1}^n \Delta SE_{\text{step}}^i(x) \equiv \Delta SE_{\text{tot}}^i(n). \quad (4)$$

In Fig. 5 the total solvation energy differences for the A and X states,  $\Delta SE_{\text{tot}}^A(n)$  and  $\Delta SE_{\text{tot}}^X(n)$ , are plotted as a function of cluster size.  $\Delta SE_{\text{tot}}^A(n)$  is essentially identical to  $\Delta SE_{\text{tot}}^-(n)$  and has therefore been omitted from the figure for

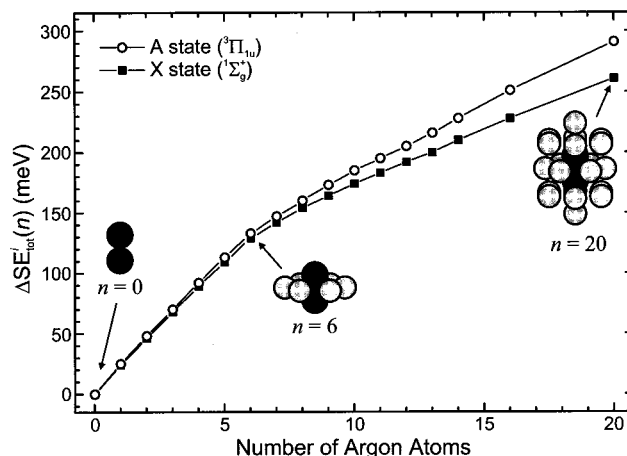


FIG. 5. Total solvation energy difference  $\Delta SE_{\text{tot}}^i(n)$  for the X and A states of  $I_2$  as a function of cluster size. Particularly stable structures [based on the molecular dynamics simulations of Faeder *et al.* (Ref. 33)] are shown for the  $n=6$  and  $n=20$  clusters.

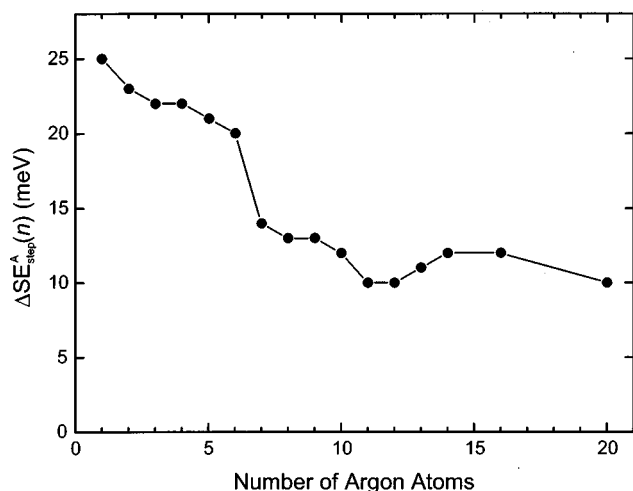


FIG. 6. Stepwise solvation energy difference  $\Delta SE_{\text{step}}^A(n)$  for the A state of  $I_2$  as a function of cluster size  $n$ .

reasons of clarity. For all states studied  $\Delta SE_{\text{tot}}^i(n)$  increases monotonically with cluster size. The increase is larger for the excited states ( $A'$  and  $A$ ).  $\Delta SE_{\text{tot}}^i(n)$  behaves close to linear in the regions from  $n=0$  to  $n=6$  and  $n=8$  to  $n=20$ , with a distinct reduction of the slope between the two regions by roughly a factor of 2. At  $n=20$ , the largest cluster studied, the anionic cluster is stabilized by 261 meV relative to the neutral cluster containing the solute in the  $X$  state and by 291 meV relative to the  $A$  state.

Trends in the solvation energies are emphasized by plotting the stepwise solvation energy difference for the  $A$  state,  $\Delta SE_{\text{step}}^A(n)$ , as a function of the cluster size  $n$  in Fig. 6. The first Ar atom is bound by 25 meV more strongly in the anion than in the neutral. From  $n=2$  to  $n=6$   $\Delta SE_{\text{step}}^A(n)$  remains nearly constant, increasing the stability of the anion relative to the neutral by an average of 22 meV per Ar atom. After  $n=6$   $\Delta SE_{\text{step}}^A(n)$  decreases considerably, first to 14 meV at  $n=7$  and then to about 11 meV for  $n=8$  to  $n=20$ . A change in  $\Delta SE_{\text{step}}^i(n)$  (Fig. 6) is manifested as a change in slope of  $\Delta SE_{\text{tot}}^i(n)$  (Fig. 5), best seen between  $n=6$  and  $n=7$ .

## V. DISCUSSION

In this section we address the shifts of the photoelectron bands upon successive solvation of  $I_2^-$ . Since we do not directly probe the solvation energy (SE) of either the anion or the neutral, but rather the difference between the two ( $\Delta SE$ ), our spectra are most sensitive to the interactions unique to either of the two species. In particular, our results reflect changes in the interaction between the charge and the added Ar atom, while they are expected to be less sensitive to contributions due to shorter range interactions, which are expected to be similar in the anion and the neutral. Comparing the  $I_2^- \cdot \text{Ar}$  spectrum to the  $I_2$  spectrum, all detachment energies are blue shifted, i.e.,  $\Delta SE_{\text{step}}^i(n)$  is positive. Thus, the Ar atom is bound more strongly in the anion than in the neutral. This behavior is expected, as the leading term in the anionic interaction is the longer range charge-induced dipole interaction term, which goes as  $r^{-4}$ , in contrast to the induced dipole-induced dipole term in the neutral, which goes as  $r^{-6}$ .

Blazy *et al.*<sup>49</sup> have determined the  $I_2 \cdot \text{Ar}$  binding energy  $D_0$  (well depth minus zero point energy) in electronically excited  $I_2(B) \cdot \text{Ar}$  by laser induced fluorescence. In combination with the observed blue shift in the absorption spectrum of  $I_2 \cdot \text{Ar}$  relative to bare  $I_2$ , they determine the  $I_2(X) \cdot \text{Ar}$  binding energy in the electronic ground state to be  $D_0(I_2 \cdot \text{Ar}) = 29.4 \pm 0.4$  meV. The  $I_2^- \cdot \text{Ar}$  binding energy can be determined by adding the solvation energy difference,  $\Delta SE_{\text{tot}}^X(1) = 24$  meV, to the binding energy of the neutral, resulting in  $D_0(I_2^- \cdot \text{Ar}) = 53 \pm 4$  meV. This value is 9 meV lower than in a recent calculation.<sup>33</sup> The discrepancy between the experimental and the theoretical values presumably results from the approximate nature of the potentials employed in the calculation. Note that the  $I_2^- \cdot \text{Ar}$  binding energy is comparable to the  $I^- \cdot \text{Ar}$  binding energy ( $D_0 = 44 \pm 2$  meV)<sup>27</sup> and only about a factor of 2 larger than the  $I_2 \cdot \text{Ar}$  binding energy. Also, we can extract  $\Delta E$  for the dissociation reaction  $I_2^- \cdot \text{Ar} \rightarrow I^- \cdot \text{Ar} + I$  from

$$\Delta E = D_0(I_2^-) + D_0(I_2^- \cdot \text{Ar}) - D_0(I^- \cdot \text{Ar}). \quad (5)$$

Using  $D_0(I_2^-) = 1.007 \pm 0.005$  eV,<sup>35</sup> we find  $\Delta E = 1.016 \pm 0.011$  eV.

We interpret the considerable reduction of  $\Delta SE_{\text{step}}^i(n)$  between  $n=6$  and  $n=7$  as a change in binding site for the subsequent Ar atoms (Fig. 6). In agreement with one of the theoretically predicted minimum energy structures<sup>33</sup> of  $I_2^- \cdot \text{Ar}_6$  we propose that the first six Ar atoms form a ring around the I–I bond (Fig. 5). The sixth Ar atom closes the ring, forcing the subsequent Ar atoms to bind closer to either one of the iodine atoms. In a simplified picture we can rationalize this, by localizing half of the charge on each iodine atom. Ar atoms in the initial ring can interact significantly with both of the partial charges, while Ar atoms located on either side will only interact strongly with the partial charge to which they are closer. From the previous ZEKE work on  $I^- \cdot \text{Ar}_n$  clusters<sup>27</sup> we know that the ion–solvent term is the leading interaction term for Ar atoms in the first solvation shell. We believe the situation to be comparable for  $I_2^- \cdot \text{Ar}_n$  clusters and therefore suggest that the ion–solvent interaction will determine the cluster geometry for the smaller clusters. A significant reduction in the ion–solvent interaction will only be partially compensated for by an increase in the solvent–solvent interaction, due to higher coordination of the Ar atoms, and thus lead to a significant reduction in  $\Delta SE_{\text{step}}^i(n)$  for  $n > 6$ . The closure of the first solvation shell around the  $I_2^-$  molecule should be indicated by a further significant reduction of  $\Delta SE_{\text{step}}^i(n)$ , due to an even larger separation between the added Ar atom and the charge. That we don't see this reduction indicates that the first solvation shell consists of at least 20 Ar atoms, consistent with the results of recent experimental and theoretical studies.<sup>28,33</sup>

The effect of the nature of the electronic state of the neutral on the solvation energy is small and below our instrumental resolution for the  $n=1$  cluster. For higher clusters, however, this effect is additive. At  $n=20$  we can tentatively state that the total solvation energy for  $I_2$  in the  $X$  state is by roughly 10% larger than in the excited states probed. This amounts to a blue shift of the  $A \leftarrow X$  transition by 30 meV in  $I_2 \cdot \text{Ar}_{20}$  relative to bare  $I_2$ . This value is identical to

the observed blue shift of the  $A \leftarrow X$  transition of  $I_2$  trapped in an argon matrix,<sup>50</sup> suggesting that the matrix limit for the solvent-induced shift of the electronic term values of  $I_2$  solvated in Ar atoms is reached at the completion of the first solvation shell.

## ACKNOWLEDGMENTS

This work has been supported by the Air Force Office of Scientific Research under Grant No. F49620-97-1-0018. K.R.A. gratefully acknowledges a postdoctoral fellowship by the Swiss National Science Foundation.

- <sup>1</sup>D. H. Levy, *Adv. Chem. Phys.* **47**, 323 (1981).
- <sup>2</sup>S. Fei, X. Zheng and M. C. Heaven, *J. Chem. Phys.* **97**, 6057 (1992).
- <sup>3</sup>M. C. R. Cockett, J. G. Goode, R. R. Maier, K. P. Lawley, and R. J. Donovan, *J. Chem. Phys.* **101**, 126 (1994).
- <sup>4</sup>E. D. Potter, Q. Liu, and A. H. Zewail, *Chem. Phys. Lett.* **200**, 605 (1992).
- <sup>5</sup>Q. Liu, J.-K. Wang, and A. H. Zewail, *Nature (London)* **364**, 427 (1993).
- <sup>6</sup>C. Lienau and A. H. Zewail, *J. Phys. Chem.* **100**, 18629 (1996).
- <sup>7</sup>Z. Li, A. Borrmann, and C. C. Martens, *J. Chem. Phys.* **97**, 7234 (1992).
- <sup>8</sup>A. Borrmann, Z. Li, and C. C. Martens, *J. Chem. Phys.* **98**, 8514 (1993).
- <sup>9</sup>X. Hu and C. C. Martens, *J. Chem. Phys.* **99**, 9532 (1993).
- <sup>10</sup>H. Schröder and H. Gabriel, *J. Chem. Phys.* **104**, 587 (1996).
- <sup>11</sup>I. Schek, J. Jortner, T. Raz, and R. D. Levine, *Chem. Phys. Lett.* **257**, 273 (1996).
- <sup>12</sup>P. Jungwirth, E. Fredj, and R. B. Gerber, *J. Chem. Phys.* **104**, 9332 (1996).
- <sup>13</sup>J.-Y. Fang and C. C. Martens, *J. Chem. Phys.* **105**, 9072 (1996).
- <sup>14</sup>A. W. Castleman and K. H. Bowen, *J. Phys. Chem.* **100**, 12911 (1996).
- <sup>15</sup>G. Markovich, S. Pollack, R. Giniger, and O. Cheshnovsky, *J. Chem. Phys.* **101**, 9344 (1994).
- <sup>16</sup>G. Markovich, S. Pollack, R. Giniger, and O. Cheshnovsky, *Z. Phys. D* **26**, 98 (1993).
- <sup>17</sup>G. Markovich, R. Giniger, M. Levin, and O. Cheshnovsky, *Z. Phys. D* **20**, 69 (1991).
- <sup>18</sup>G. Markovich, R. Giniger, M. Levin, and O. Cheshnovsky, *J. Chem. Phys.* **95**, 9416 (1991).
- <sup>19</sup>S. T. Arnold, J. H. Hendricks, and K. H. Bowen, *J. Chem. Phys.* **102**, 39 (1995).
- <sup>20</sup>A. Furlan, T. Troxler, and S. Leutwyler, *J. Phys. Chem.* **97**, 13527 (1993).
- <sup>21</sup>M. Schmidt, M. Mons, and J. Le Calvé, *Chem. Phys. Lett.* **177**, 371 (1991).
- <sup>22</sup>U. Even, N. Ben-Horin, and J. Jortner, *Phys. Rev. Lett.* **62**, 140 (1989).
- <sup>23</sup>P. D. Dao, S. Morgan, and A. W. Castleman, *Chem. Phys. Lett.* **113**, 219 (1985).
- <sup>24</sup>D. W. Arnold, S. E. Bradforth, E. H. Kim, and D. M. Neumark, *J. Chem. Phys.* **102**, 3510 (1995).
- <sup>25</sup>D. W. Arnold, S. E. Bradforth, E. H. Kim, and D. M. Neumark, *J. Chem. Phys.* **102**, 3493 (1995).
- <sup>26</sup>D. W. Arnold, S. E. Bradforth, E. H. Kim, and D. M. Neumark, *J. Chem. Phys.* **97**, 9468 (1992).
- <sup>27</sup>I. Yourshaw, Y. X. Zhao, and D. M. Neumark, *J. Chem. Phys.* **105**, 351 (1996).
- <sup>28</sup>V. Vorsa, P. J. Campagnola, S. Nandi, M. Larsson, and W. C. Lineberger, *J. Chem. Phys.* **105**, 2298 (1996).
- <sup>29</sup>V. Vorsa, S. Nandi, P. J. Campagnola, M. Larsson, and W. C. Lineberger, *J. Chem. Phys.* **106**, 1402 (1997).
- <sup>30</sup>B. J. Greenblatt, M. T. Zanni, and D. M. Neumark, *Chem. Phys. Lett.* **258**, 523 (1996).
- <sup>31</sup>B. J. Greenblatt, M. T. Zanni, and D. M. Neumark, *Science* **276**, 1675 (1997).
- <sup>32</sup>V. S. Batista and D. F. Coker, *J. Chem. Phys.* **106**, 7102 (1997).
- <sup>33</sup>J. Faeder, N. Delaney, P. E. Maslen, and R. Parson, *Chem. Phys. Lett.* **270**, 196 (1997).
- <sup>34</sup>J. Faeder and R. Parson, *J. Chem. Phys.* **108**, 3909 (1998).
- <sup>35</sup>J. M. Papanikolas, J. R. Gord, N. E. Levinger, D. Ray, V. Vorsa, and W. C. Lineberger, *J. Phys. Chem.* **95**, 8028 (1991).
- <sup>36</sup>J. M. Papanikolas, V. Vorsa, M. E. Nadal, P. J. Campagnola, J. R. Gord, and W. C. Lineberger, *J. Chem. Phys.* **97**, 7002 (1992).
- <sup>37</sup>J. M. Papanikolas, V. Vorsa, M. E. Nadal, P. J. Campagnola, H. K. Buchenau, and W. C. Lineberger, *J. Chem. Phys.* **99**, 8733 (1993).
- <sup>38</sup>D. Ray, N. E. Levinger, J. M. Papanikolas, and W. C. Lineberger, *J. Chem. Phys.* **91**, 6533 (1989).
- <sup>39</sup>M. L. Alexander, N. E. Levinger, M. A. Johnson, D. Ray, and W. C. Lineberger, *J. Chem. Phys.* **88**, 6200 (1988).
- <sup>40</sup>M. T. Zanni, T. R. Taylor, B. J. Greenblatt, B. Soep, and D. M. Neumark, *J. Chem. Phys.* **107**, 7613 (1997).
- <sup>41</sup>R. B. Metz, A. Weaver, S. E. Bradforth, T. N. Kitsopoulos, and D. M. Neumark, *J. Phys. Chem.* **94**, 1377 (1990).
- <sup>42</sup>C. Xu, G. R. Burton, T. R. Taylor, and D. M. Neumark, *J. Chem. Phys.* **107**, 3428 (1997).
- <sup>43</sup>K. S. Viswanathan and J. Tellinghuisen, *J. Mol. Spectrosc.* **101**, 285 (1983).
- <sup>44</sup>J. Tellinghuisen, *J. Chem. Phys.* **82**, 4012 (1985).
- <sup>45</sup>C. Teichteil and M. Pelissier, *Chem. Phys.* **180**, 1 (1994).
- <sup>46</sup>F. Martin, R. Bacis, S. Churassy, and J. Verges, *J. Mol. Spectrosc.* **116**, 71 (1986).
- <sup>47</sup>X. N. Zheng, S. L. Fei, M. C. Heaven, and J. Tellinghuisen, *J. Chem. Phys.* **96**, 4877 (1992).
- <sup>48</sup>D. R. T. Appadoo, R. J. Leroy, P. F. Bernath, S. Gerstenkorn, P. Luc, J. Verges, J. Sinzelle, J. Chevillard, and Y. Daignaux, *J. Chem. Phys.* **104**, 903 (1996).
- <sup>49</sup>J. A. Blazy, B. M. DeKoven, T. D. Russell, and D. H. Levy, *J. Chem. Phys.* **72**, 2439 (1980).
- <sup>50</sup>M. Macler and M. Heaven, *Chem. Phys.* **151**, 219 (1991).